Descent Angle Control by Regenerative Air Brake Using Observer-based Thrust Control for Electric Aircraft

Kentaro Yokota *, Hiroshi Fujimoto † and Yoichi Hori ‡
The University of Tokyo, Kashiwa, Chiba, 277-8561

Research and development have been very active in electric aircraft (EA). EA use electric motors as the power source; therefore, EA are expected to achieve more secure, more efficient, and more eco-friendly aviation. Electric motors enable EA to regenerate their potential energy while descending as the windmilling propeller produces negative torque and thrust. This paper proposes descent angle control method by using windmilling propeller as an alternative to mechanical air brakes. In addition, the use of wide range of propeller pitch angle is discussed in order to produce enough drag to eliminate mechanical air brakes. The effectiveness of the proposed method is verified by simulations and experiments in the wind tunnel.

I. Nomenclature

α, α_0	=	perturbation variables of angle of attack, trim angle of attack [rad]
β	=	propeller pitch angle [deg]
δ_{ab}	=	deflection angle of air brakes [rad]
δ_{t}	=	throttle setting [−]
θ, Θ_0	=	perturbation variables of pitch angle, pitch angle of aircraft [rad, deg]
ρ	=	air density [$\mathrm{kg\,m^{-3}}$]
m	=	mass of aircraft [kg]
n	=	rotational speed of propeller [rps]
q	=	perturbation variables of pitch rate [$\mathrm{rad\,s^{-1}}$]
u, U_0	=	perturbation variables of velocity of x axis, trim velocity of x axis [$\mathrm{m\,s^{-1}}$]
D_ω	=	viscosity coefficient of motor [$\mathrm{N\,m\,s\,rad^{-1}}$]
C_L	=	lift coefficient of aircraft [−]
C_D	=	drag coefficient of aircraft [−]
C_F	=	thrust coefficient of propeller [−]
C_Q	=	torque coefficient of propeller [−]
D	=	drag of aircraft [N]
D_p	=	propeller diameter [m]
F, F_0, ΔF	=	propeller thrust, trim thrust, thrust change from trim [N]
I_{yy}	=	inertia moment of aircraft [$\mathrm{kg\,m^2}$]
J	=	advance ratio [−]
J_ω	=	inertia moment of propeller [$\mathrm{kg\,m^2}$]
L	=	lift of aircraft [N]
Q	=	counter torque of propeller [N m]
S	=	area of wing [$\mathrm{m^2}$]
T	=	input toque of motor [N m]
T_C	=	coulomb friction of motor [N m]
V	=	airspeed [$\mathrm{m\,s^{-1}}$]
$X_u, Z_u, M_u, X_\alpha, Z_\alpha, M_\alpha, M_{\dot{\alpha}}, X_q, Z_q, M_q$	=	stability derivatives
$X_{\delta_{\mathrm{ab}}}, Z_{\delta_{\mathrm{ab}}}, M_{\delta_{\mathrm{ab}}}, X_{\delta_{\mathrm{t}}}, Z_{\delta_{\mathrm{t}}}, M_{\delta_{\mathrm{t}}}$	=	control derivatives

*Student, Department of Electrical and Electronic Engineering, The University of Tokyo, IEEE Student Member, AIAA Student Member.
†Associate Professor, Graduate School of Frontier Science, The University of Tokyo, IEEE Senior Member.
‡Professor, Graduate School of Frontier Science, The University of Tokyo, IEEE Fellow.

II. Introduction

A. Eleric Aircraft

Over the past few years, the demand for personal and eco-friendly aviation has increased. Accordingly, several studies have been conducted on electric aircraft (EA) [1]. As EA are powered by electric motors, they have the following advantages:

1) Motor torque generation is 100 times faster than that of internal combustion engines [2].
2) Motor torque measurement is accurate [2].
3) Distributed installation and independent control of motors are easy [3].
4) Power regeneration is feasible [4].

These advantages enable EA to be more secure, more efficient, and more eco-friendly aviation.

The authors' research group has proposed a quick thrust control method [5] and range extension systems [6][7] by adopting the motion control theories developed in the automotive industry [8].

B. Power Regeneration by Propellers

Previous studies showed that the windmilling propeller allows the motor to generate electric power [4][9][10][11][12]. A propeller in the windmill state produces negative thrust and negative torque; therefore, EA can regenerate about 10% of their potential energy while descending [4]. Additionally, the energy generated during descent allows an EA to cruise about 60% of the descent distance at most [9]. Regeneration during descent reduces the batteries for the descent, loiter, go-around, and taxiing.

In [12], the concept of regenerative air brake which enables descent without using mechanical air brakes was proposed and demonstrated in the flight tests. This method uses the negative thrust of the windmilling propeller as the substitute for mechanical air brakes. The pilot can control the descent rate without the mechanical air brakes, but since the pilot can only change the motor torque, the operation mainly depends on the ability of the pilot. In addition, the negative thrust the windmilling propeller produces is not large enough to eliminate the mechanical air brakes in order to follow the guideline of motor gliders.

C. About This Paper

This paper focuses on the control of the descending airplane. The conventional method uses mechanical air brakes such as spoiler to adjust the descent angle; however, since they cannot be controlled continuously, even a skilled pilot finds it difficult to operate the brakes [11]. The airfield usually requests the top of descent (TOD) and the bottom of descent (BOD), but due to this difficulty, the conventional airplane descends a zigzag path, as shown in Fig. 1.

The purpose of this study is to discuss the control performance of regenerative air brake, and achieve descent angle control in the regenerative area. The proposed method includes observer-based airspeed estimation, thrust estimation observer, negative thrust control, and descent angle control. In addition, the use of wide range of propeller pitch angle is discussed to produce enough negative thrust to follow the motor glider guideline.

This paper is organized as follows: Section III describes the modeling of a single motor EA, and Section IV describes the experimental setup. The observer-based airspeed estimation, thrust estimation observer, negative thrust control are explained in Section V, and the descent angle controller is designed in Section VI. Finally, the use of various propeller pitch angle is discussed in Section VII.

III. Modeling of Single Motor Electric Aircraft

In this section, a single motor EA is modeled.

A. Aircraft Dynamics [10]

Fig. 2(a) shows a view of the aircraft in a steady descent. The vector sum of all forces is zero since the aircraft is in equilibrium. Hence, in the direction of descent,

$$F\cos\alpha_0 + mg\sin(\Theta_0 + \alpha_0) - D = 0. \tag{1}$$

Normal to this direction,

$$L + F\sin\alpha_0 - mg\cos(\Theta_0 + \alpha_0) = 0. \tag{2}$$

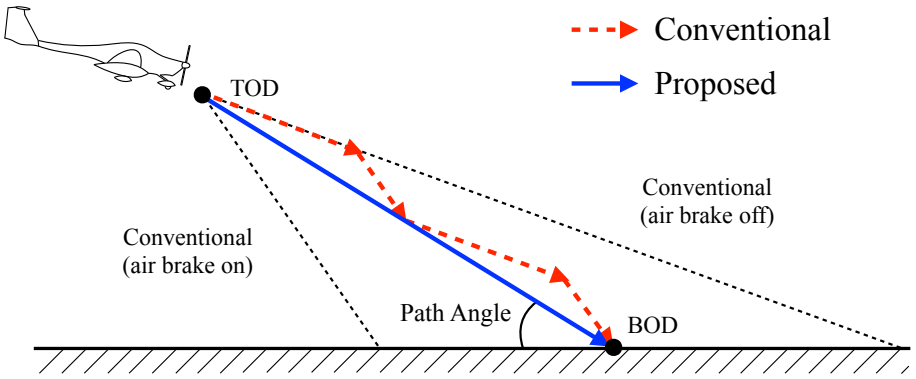

Fig. 1 The conventional and proposed descent paths [11].

These equations can be solved for Θ_0 to give

$$\tan(\Theta_0 + \alpha_0) = \frac{D - F\cos\alpha_0}{L + F\sin\alpha_0}. \tag{3}$$

L and D are given by

$$L = \frac{1}{2}\rho C_L S V^2, \tag{4}$$

$$D = \frac{1}{2}\rho C_D S V^2. \tag{5}$$

L and D are constant under constant ρ and V; therefore, Θ becomes a function of only F.

The state-space equation of vertical motion is as follows:

$$\dot{\boldsymbol{x}} = \boldsymbol{A}\boldsymbol{x} + \boldsymbol{B}\boldsymbol{u}, \tag{6}$$

$$\boldsymbol{x} = \begin{bmatrix} u \\ \alpha \\ q \\ \theta \end{bmatrix}, \tag{7}$$

$$\boldsymbol{u} = \begin{bmatrix} \delta_{\mathrm{ab}} \\ \delta_{\mathrm{t}} \end{bmatrix}, \tag{8}$$

$$\boldsymbol{A} = \begin{bmatrix} X_u & X_\alpha & X_q - W_0 & -g\cos\Theta_0 \\ Z_u/U_0 & Z_\alpha/U_0 & Z_q/U_0 + 1 & -g\sin\Theta_0/U_0 \\ M_u + M_{\dot{\alpha}}\left(Z_u/U_0\right) & M_\alpha + M_{\dot{\alpha}}\left(Z_\alpha/U_0\right) & M_q + M_{\dot{\alpha}}\left(Z_q/U_0 + 1\right) & -M_{\dot{\alpha}} g\sin\Theta_0/U_0 \\ 0 & 0 & 1 & 0 \end{bmatrix}, \tag{9}$$

$$\boldsymbol{B} = \begin{bmatrix} X_{\delta_{\mathrm{ab}}} & X_{\delta_{\mathrm{t}}} \\ Z_{\delta_{\mathrm{ab}}}/U_0 & Z_{\delta_{\mathrm{t}}}/U_0 \\ M_{\delta_{\mathrm{ab}}} + M_{\dot{\alpha}}\left(Z_{\delta_{\mathrm{e}}}/U_0\right) & M_{\delta_{\mathrm{t}}} + M_{\dot{\alpha}}\left(Z_{\delta_{\mathrm{t}}}/U_0\right) \\ 0 & 0 \end{bmatrix}. \tag{10}$$

Let ΔF be the thrust change from the trim. If ΔF is the only control input, $\boldsymbol{u}$ and $\boldsymbol{B}$ becomes

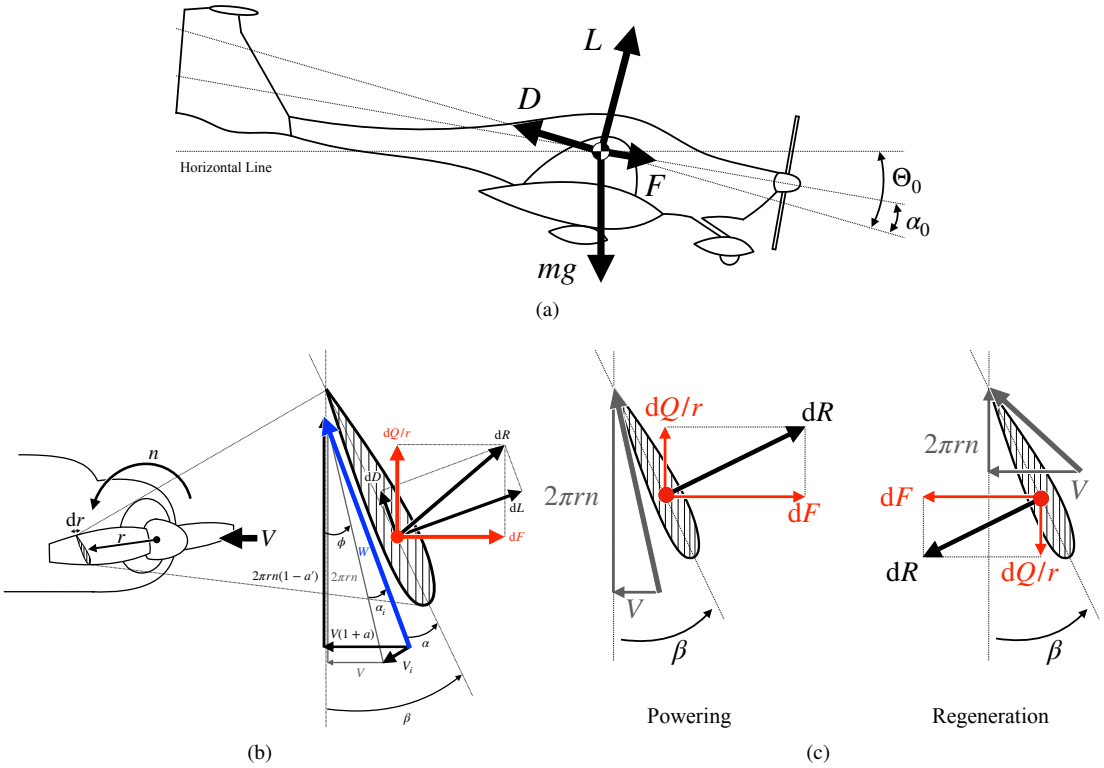

Fig. 2 (a) A view of the aircraft in a steady descent. (b) Velocities and forces acting on the propeller blade element. (c) A view of the powering propeller (left) and windmilling propeller (right).

$$\boldsymbol{u} = \Delta F, \tag{11}$$

$$\boldsymbol{B} = \begin{bmatrix} \frac{1}{m} \\ 0 \\ 0 \\ 0 \end{bmatrix}. \tag{12}$$

Therefore, the transfer function of the system regarding the pitch angle is given by

$$\frac{\theta}{\Delta F} = \begin{bmatrix} 0 & 0 & 0 & 1 \end{bmatrix} (s\boldsymbol{I} - \boldsymbol{A})^{-1} \begin{bmatrix} \frac{1}{m} \\ 0 \\ 0 \\ 0 \end{bmatrix}. \tag{13}$$

B. Propeller Dynamics [10, 13]

A propeller-driven aircraft obtains all of its thrust from the propeller. Fig. 2(b) shows velocities and forces acting on the propeller blade element. V_i is the induced velocity, $\mathrm{d}L$ is the differential lift, and $\mathrm{d}D$ is the differential drag. The contribution of the blade element to F and Q is

$$\mathrm{d}F = \mathrm{d}L \cos(\phi + \alpha_i) - \mathrm{d}D \sin(\phi + \alpha_i), \tag{14}$$

$$\mathrm{d}Q/r = \mathrm{d}L \sin(\phi + \alpha_i) + \mathrm{d}D \cos(\phi + \alpha_i). \tag{15}$$

Similar to (4) and (5), $\mathrm{d}L$ and $\mathrm{d}D$ can be calculated by

$$\mathrm{d}L = \frac{1}{2}\rho C_L c \mathrm{d}r W^2, \tag{16}$$

$$\mathrm{d}D = \frac{1}{2}\rho C_D c \mathrm{d}r W^2, \tag{17}$$

where c is the chord. Let B be the number of the blades, then

$$F = B\int \mathrm{d}F = B\int \left\{\mathrm{d}L\cos\left(\phi+\alpha_i\right) - \mathrm{d}D\sin\left(\phi+\alpha_i\right)\right\}, \tag{18}$$

$$Q = B\int \mathrm{d}Q = B\int r\left\{\mathrm{d}L\sin\left(\phi+\alpha_i\right) + \mathrm{d}D\cos\left(\phi+\alpha_i\right)\right\}. \tag{19}$$

Considering the theoretical equations (16)–(19), C_F and C_Q are defined from experimental results as follows:

$$C_F = \frac{F}{\rho n^2 D_p^4}, \tag{20}$$

$$C_Q = \frac{Q}{\rho n^2 D_p^5}. \tag{21}$$

From Fig. 2(b), the angle of resultant flow ϕ is determined by the ratio of V and $2\pi nr$.

$$\tan\phi = \frac{V}{2\pi nr} = \frac{J}{\pi\frac{2r}{D_p}}. \tag{22}$$

J is called the advance ratio and defined by

$$J = \frac{V}{nD_p}. \tag{23}$$

Thus, C_F and C_Q are functions of J. F and Q can be written as

$$F = C_F(J)\rho n^2 D_p^4, \tag{24}$$

$$Q = C_Q(J)\rho n^2 D_p^5. \tag{25}$$

Fig. 2(c) shows a view of the powering propeller (left) and windmilling propeller (right). As the figure shows, if the directions of F and Q are assumed to be positive when powering, the propeller in the windmilling state produces negative F and Q. In other words, C_F and C_Q become negative at high J.

The equation of motion of electric motor is

$$T - Q = 2\pi J_\omega \frac{\mathrm{d}n}{\mathrm{d}t} + 2\pi B_\omega n + T_C. \tag{26}$$

Ignoring the friction of the motor in (26), the input power P is calculated by

$$P = 2\pi nT = 2\pi nQ. \tag{27}$$

P becomes negative when Q is negative, enabling power regeneration. Also, from (3), the negative thrust allows a wide range of Θ.

IV. Experimental Setup

A diagram and a picture of the experimental setup are shown in Fig. 3(a)–Fig. 3(b). The experimental unit consists of a linear guide, a load cell, a motor, an encoder, an APC propeller 8×4, a pitot tube, and a wind tunnel. The load cell measures F, the encoder measures n, and the pitot tube measures V.

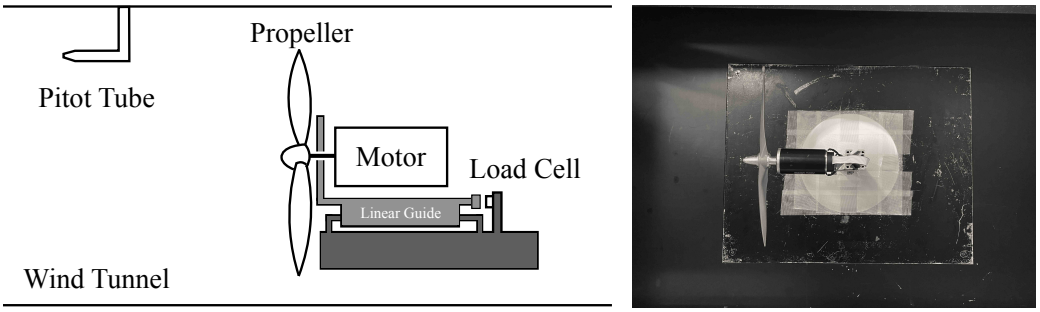

(a) (b)

Fig. 3 (a) A diagram of of the experimental setup. (b) A picture of the experimental setup.

Tab. 1 Experiment parameters.

Parameter	Value	Unit
inertia moment J_ω	1.29×10^{-4}	$\mathrm{kg\,m^2}$
viscosity coefficient B_ω	4.32×10^{-6}	$\mathrm{N\,m\,s\,rad^{-1}}$
coulomb friction T_C	2.48×10^{-3}	$\mathrm{N\,m}$

V. Thrust Control

In this section, observer-based airspeed estimation method, thrust estimation observer, and negative thrust control are proposed.

The propeller thrust control method is proposed in [5], and adopted to windmilling propeller [14] as shown in Fig. 4(a). In order to achieve quick control of the propeller thrust, airspeed measurement should be faster than conventional pitot tubes, which have poor response. Also, the thrust must be estimated since adding force sensors decreases the stiffness of the thrusters.

The idea of V estimation from motor torque is suggested in [15], and adopted to the authors' observer-based estimation scheme [14]. The counter torque Q can be estimated by the counter torque observer shown in Fig. 4(c). By using (23), (25), and the estimated value of Q, V can be estimated as follows:

$$\hat{V} = nD_p C_Q^{-1}\left(\frac{\hat{Q}}{\rho n^2 D_p^5}\right). \tag{28}$$

Since the motor torque has a quick response, V can be estimated faster than the conventional pitot tube. The step response of V is shown in Fig. 5(a). Note that only the rotational speed of the wind tunnel fan was changed stepwise at $t = 4\,\mathrm{s}$, and the actual change of the airspeed can not be measured. As seen in Fig. 5(a), by using the counter torque observer, V can be estimated about five times faster than pitot tube. This quick estimation enables quick thrust control.

The basic idea of the thrust estimation observer (TEO) is similar to the airspeed estimation scheme. Fig. 4(c) shows the overview of TEO. In $F(Q, n)$, $\hat{F}$ is calculated by (24) and (25). There are several ways to obtain $\hat{F}$, but the proposed method uses the linear relation between C_F and C_Q as shown in Fig. 5(b). Thus,

$$C_F = aC_Q + b, \tag{29}$$

$$\hat{F} = a\frac{\hat{Q}}{D_p} + b\rho n^2 D_p^4. \tag{30}$$

The negative thrust controller is designed as a two-degree-of-freedom control and uses the estimated thrust $\hat{F}$ in the feedback controller. Fig. 4(a) shows the block diagram of the controller. The effectiveness of TEO and negative thrust control is verified by a simulation and wind tunnel test.

The simulation model uses the parameter of APC propeller 11×5.5 propeller. D_ω and T_c are assumed to be zero in this simulation.

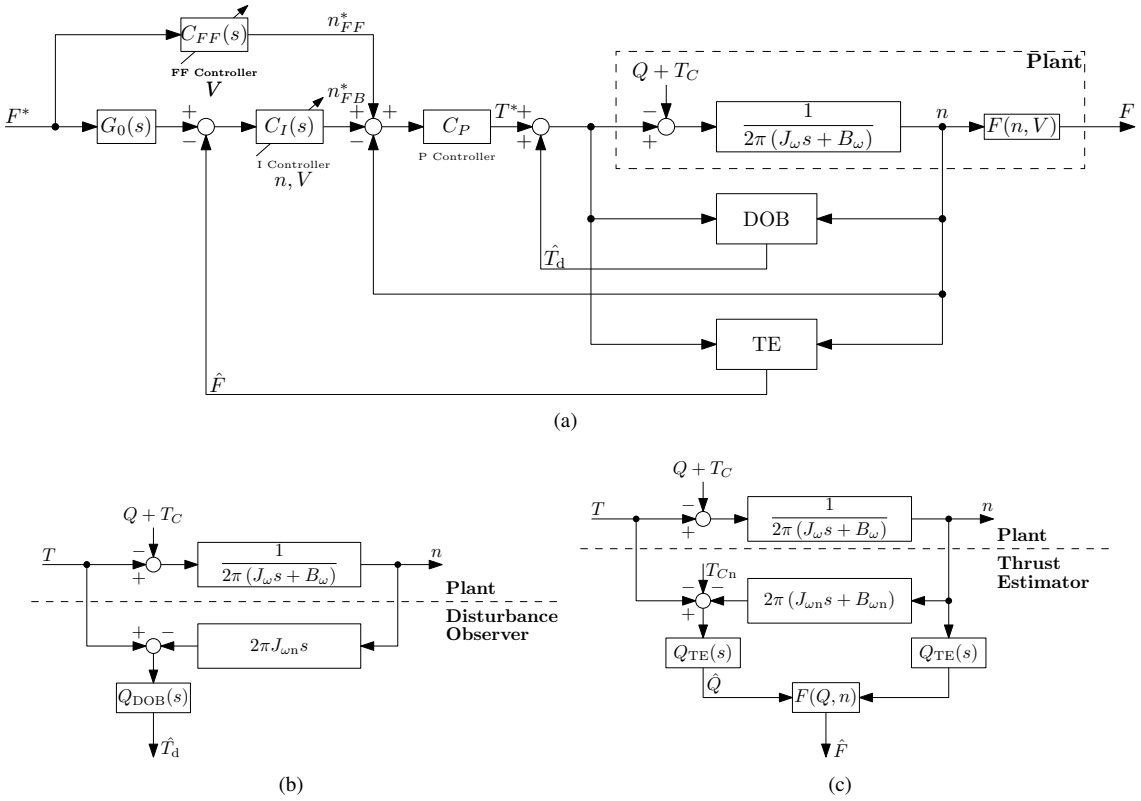

Fig. 4 (a) Negative thrust controller using thrust estimation observer [14]. (b) Disturbance observer (DOB). (c) Thrust estimation observer (TEO).

The step response and the tailwind disturbance response are shown in Fig. 5(c). $\hat{F}$ is the estimated thrust, which is controller feedback. F is the real value. V was $7\,\mathrm{m\,s^{-1}}$. The thrust reference was exponentially changed from -1 N to -1.2 N at $t = 1$ s, and V was changed to $6\,\mathrm{m\,s^{-1}}$ at $t = 4$ s. Fig. 5(c) shows that the proposed method achieved the quick responses to both reference change and tailwind disturbance. The result also indicates the effectiveness of the thrust estimation as the maximum error is 0.42%.

Fig. 5(d) shows the step response of F. The thrust reference was exponentially changed from -0.82 N to -1.32 N at $t = 2$ s. $\hat{F}$ is the output of the thrust estimation observer, which is the controller feedback. F is the real value of the thrust measured by the load cell. Fig. 5(d) shows that the thrust estimation observer achieved accurate estimation, and the negative thrust controller achieved a quick response.

VI. Descent Angle Control

In this section, the descent angle control method is proposed. This method is unique in that only thrust is used to control the pitch angle. Conventional aircraft usually use mechanical air brakes or elevators to change the descent angle, and the thrust is not used actively to control the attitude. However, by taking advantage of electric motors, EA can actively change their thrust. Therefore, the proposed negative thrust control enables not only power regeneration but also high control performance of their attitude.

The block diagram of the descent angle (pitch angle) controller is Fig. 6. Note that this paper focuses on the pitch control, and an outer loop should be added to control the descent path. The proposed method consists of a pitch rate controller and a pitch angle controller.

The remainder of this section focuses on the controller design and the simulation of the proposed method for Diamond Aircraft HK–36 TTC ECO. The picture of HK–36 TTC ECO is shown in Fig. 7, and the simulation parameters are shown in Table 2. These parameters were theoretically estimated from flight tests [16–18]. The estimation formulas

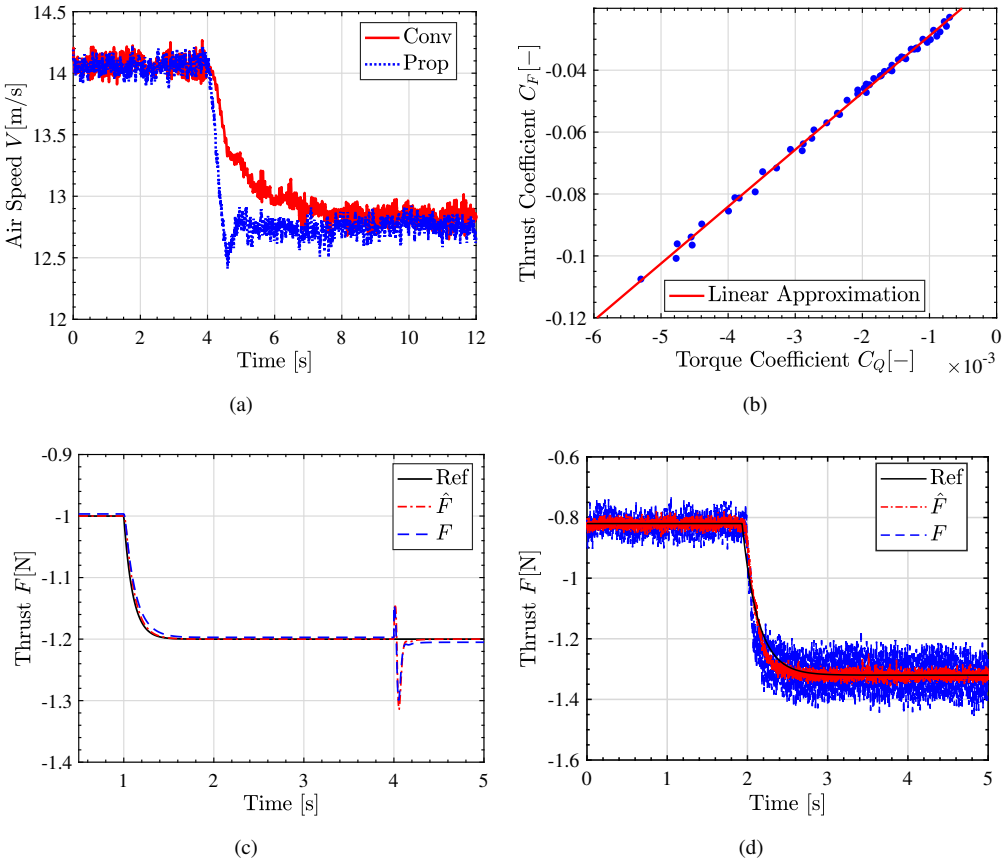

Fig. 5 (a) Step response of V. (b) The relation between C_Q and C_F of windmilling APC propeller 11×5.5 [4]. (c) The simulation result of step response and tailwind disturbance response of F. (d) The wind tunnel test result of step response of F.

are shown in Table 3 [19]. α_0 was assumed to be very small. From (13) and Table 2, the transfer function of the plant is

$$\frac{\theta}{\Delta F} = \frac{1.58 \times 10^{-5} s + 1.25 \times 10^{-4}}{s^4 + 3.96 s^3 + 7.56 s^2 + 7.88 \times 10^{-1} s + 9.78 \times 10^{-1}}. \tag{31}$$

A. Pitch Rate Controller

The pitch rate controller is a PD controller using a disturbance observer. The control input of the pitch rate controller goes to the negative thrust controller shown in Fig. 4(a). Regarding ΔF^* and ΔF,

$$F^* = F_0 + \Delta F^*, \tag{32}$$

$$F = F_0 + \Delta F. \tag{33}$$

First, disturbance observer was used to nominalize the plant to $P_\mathrm{n}(s)$ [21]. From (31), the transfer function of the real plant from ΔF to q is

$$P(s) = \frac{q}{\Delta F} = \frac{1.58 \times 10^{-5} s^2 + 1.25 \times 10^{-4} s}{s^4 + 3.96 s^3 + 7.56 s^2 + 7.87 \times 10^{-1} s + 9.73 \times 10^{-1}}. \tag{34}$$

The transfer function of the nominal plant is

$$P_\mathrm{n}(s) = \frac{1.58 \times 10^{-5}}{s^2}. \tag{35}$$

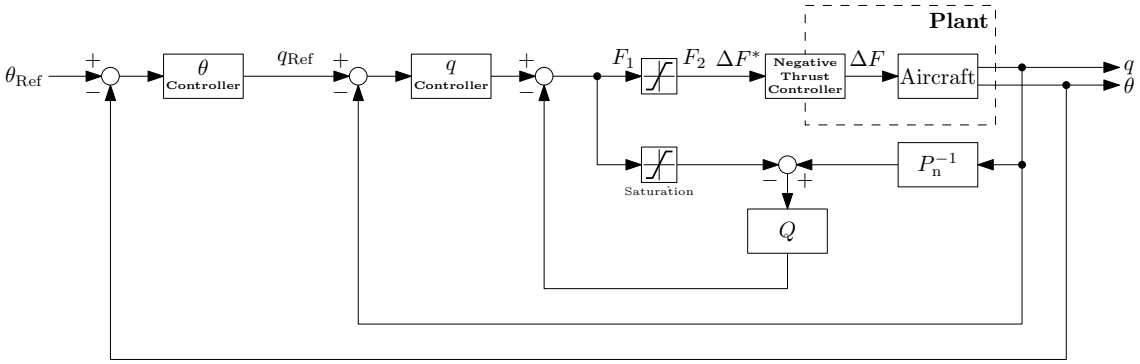

Fig. 6 Descent angle (pitch angle) controller.

Fig. 7 Diamond Aircraft HK–36 TTC ECO [20].

However, since the negative thrust has a lower limit depending on airspeed, anti-windup has to be considered. This is a critical issue of the regenerative air brake. Therefore, a saturation was placed in the disturbance observer as shown in Fig. 6. The calculation of the lower limit is as follows. First, apply a linear approximation to the relation between J and C_F.

$$C_F = a_{CF}J + b_{CF}, \tag{36}$$

$$\therefore F = (a_{CF}J + b_{CF})\,\rho n^2 D_p^4 = a_{CF}\rho D_p^3 V n + b_{CF}\rho n^2 D_p^4. \tag{37}$$

Then, calculate the value of $n_{\min}$ where F is minimized at constant V.

$$\left.\frac{\partial F}{\partial n}\right|_{n=n_{\min}} = 0, \tag{38}$$

$$\therefore n_{\min} = \frac{-a_{CF}}{2b_{CF}D_p}V. \tag{39}$$

Note that a_{CF} is a negative value. Finally, calculate the thrust lower limit $F_{\min}$ from $n_{\min}$.

$$F_{\min} = a_{CF}\rho D_p^3 V n_{\min} + b_{CF}\rho n_{\min}^2 D_p^4. \tag{40}$$

The upper limit is determined by the specification of the motor.

The PD controller was designed to the nominal model $P_{\mathrm{n}}(s)$, and the poles were placed at

$$\omega_q = 10\,\mathrm{rad\,s^{-1}}. \tag{41}$$

B. Pitch Angle Controller

The pitch angle controller is a proportional controller. If the pitch rate controller is fast enough, the transfer function from q to θ is

$$\frac{\theta}{q} = \frac{1}{s}. \tag{42}$$

Tab. 2 Diamond Aircraft HK–36 TTC ECO parameters.

Parameter	Value	Unit
mass m	8.00×10^2	N
wing area S	1.53×10	m^2
wing span	1.63×10	m
length	7.28	m
propeller diameter D_p	1.75	m
inertia I_{yy}	1.60×10^3	$kg\,m^2$
chord c	1.00	m
air density ρ	1.20	$kg\,m^{-3}$
trim pitch angle Θ_0	−3.00	deg
trim velocity U_0	3.00×10	$m\,s^{-1}$
trim thrust F_0	1.48×10	N
X_u	-3.54×10^{-2}	s^{-1}
Z_u	-6.52×10^{-1}	s^{-1}
M_u	0	$m^{-1}\,s^{-1}$
X_α	8.07	$m\,s^{-2}$
Z_α	-4.45×10	$m\,s^{-2}$
M_α	−4.58	s^{-2}
$M_{\dot{\alpha}}$	-5.82×10^{-1}	s^{-1}
X_q	0	$m\,s^{-1}$
Z_q	-8.87×10^{-1}	$m\,s^{-1}$
M_q	−1.88	s^{-1}

The poles was placed at

$$\omega_\theta = 1\,\mathrm{rad\,s^{-1}}. \tag{43}$$

C. Simulation

A simulation verified the proposed method using the parameters of Diamond Aircraft HK–36 TTC ECO. The simulation considered a descending aircraft; therefore, the trim pitch angle was set to −3 deg at $U_0 = 3.00 \times 10\,\mathrm{m\,s^{-1}}$ and $F_0 = 1.48 \times 10\,\mathrm{N}$.

The simulation results are Fig. 8(a)–Fig. 8(d). Fig. 8(a) shows the step response of the pitch angle, Fig. 8(b) shows the reference and output of the pitch rate controller, and Fig. 8(c) shows the control input. As seen in Fig. 8(a), the response is quick enough for an aircraft. Also, in Fig. 8(c), the control input was saturated, meaning the anti-windup controller is indispensable.

The comparison of the proposed method and the conventional air brakes is shown in Fig. 8(d).

Fig. 8(d) shows the descent path of the proposed and conventional methods. The proposed method uses the descent angle controller, and the conventional method uses the mechanical air brakes. The control derivatives of the mechanical were estimated from the flight test [16]. The mechanical air brakes change the airfoil and reduce L/D. When the mechanical air brakes were half opened, the L/D is reduced to 10.54, and when fully opened, it is reduced to 7.17.

Since the mechanical air brakes usually do not have their actuators, only the choices of open, half-opened, and closed are available. Thus, in the simulation, they are half-opened when the aircraft is at a certain distance from the target path and closed when it is on the target path. To be more specific, the mechanical air brakes were half-opened at $X_e = 0.9\,\mathrm{m}$, and closed at $X_e = 1.65\,\mathrm{m}$.

The conventional method descends a zigzag path because the mechanical air brakes cannot be controlled continually. However, the proposed method takes advantage of electric motors' high control performance and follows the target path.

Tab. 3 Estimation and transformation formulas of stability derivatives [19].

Non-dimensional Stability Derivative	Estimation Formula	Stability Derivative	Transformation Formula
C_{x_u}	$-2\left(C_L \tan\Theta_0 + C_D\right)$	X_u	$\frac{\rho U_0 S}{2M}\left(C_{x_u} + 2C_L \tan\Theta_0\right)$
C_{z_u}	0	Z_u	$\frac{\rho U_0 S}{2M}\left(C_{z_u} - 2C_L\right)$
C_{m_u}	0	M_u	$\frac{\rho U_0 S\bar{c}}{2I_{yy}} C_{m_u}$
C_{x_α}	$C_L\left(1 - \frac{2C_{L_\alpha}}{\pi e A}\right)$	X_α	$\frac{\rho U_0^2 S}{2M}\left(C_{x_\alpha} + 2C_L \tan\alpha_0 \tan\Theta_0\right)$
C_{z_α}	$-C_{L_\alpha}$	Z_α	$\frac{\rho U_0^2 S}{2M}\left(C_{z_\alpha} - 2C_L \tan\alpha_0\right)$
C_{m_α}	$a_\mathrm{w}\left\{(h - h_\mathrm{nw}) - V_\mathrm{h}^* \frac{a_\mathrm{t}}{a_\mathrm{w}}\left(1 - \left[\frac{\partial\varepsilon}{\partial\alpha}\right]_0\right) + V_\mathrm{fus}^* \frac{2}{a_\mathrm{w}}\right\}$	M_α	$\frac{\rho U_0^2 S\bar{c}}{2I_{yy}} C_{m_\alpha}$
$C_{m_{\dot{\alpha}}}$	$-2V_\mathrm{h}^* \frac{l_\mathrm{t}}{\bar{c}} a_\mathrm{t}\left[\frac{\partial\varepsilon}{\partial\alpha}\right]_0$	$M_{\dot{\alpha}}$	$\frac{\rho U_0 S\bar{c}^2}{4I_{yy}} C_{m_{\dot{\alpha}}}$
C_{x_q}	0	X_q	$\frac{\rho U_0 S\bar{c}}{4M} C_{x_q}$
C_{z_q}	$-2V_\mathrm{h}^* a_\mathrm{t}$	Z_q	$\frac{\rho U_0 S\bar{c}}{4M} C_{z_q}$
C_{m_q}	$-2V_\mathrm{h}^* \frac{l_\mathrm{t}}{\bar{c}} a_\mathrm{t}$	M_q	$\frac{\rho U_0 S\bar{c}^2}{4I_{yy}} C_{m_q}$
C_{L_α}	$a_\mathrm{w}\left\{1 + \frac{a_\mathrm{t}}{a_\mathrm{w}}\frac{S_\mathrm{t}}{S}\left(1 - \left[\frac{\partial\varepsilon}{\partial\alpha}\right]_0\right)\right\}$		

VII. Various Propeller Pitch Angle

[12] attempted to use windmilling propeller as a substitute of mechanical air brakes. However, [12] concludes that the mechanical air brakes can not be eliminated since the negative thrust is not large enough to follow the motor glider guideline. The wight and drag of the glider are about 8000 N and 400 N. The negative thrust at constant pitch angle is about 300 N; therefore, the lift–drag ratio L/D can be reduced to about 11. However, according to the guideline of motor gliders, L/D must be lower than 7 when all the brakes are on. In order to solve this problem, the use of wide range of propeller pitch angle β should be discussed by using variable pitch propeller. Hereafter, β_0 is the constant pitch angle when cruising, and $\Delta\beta$ is defined as the difference from β_0 in the direction where β increases. Therefore,

$$\beta = \beta_0 + \Delta\beta. \tag{44}$$

Propeller characteristics at $\Delta\beta = 180$ deg, which have never been discussed, are measured. Hereafter, $\Delta\beta = 0$ deg is called normal pitch, and $\Delta\beta = 180$ deg is called opposite pitch. The relations between n and F of APC 8×4 normal pitch at $V = 5.6\,\mathrm{m\,s^{-1}}$ is compared to that of opposite pitch in Fig. 9(a). Also, the relations between n and P of APC 8×4 normal pitch at $V = 5.6\,\mathrm{m\,s^{-1}}$ is compared to that of opposite pitch in Fig. 9(b). As shown in Fig. 9, the opposite pitch produces about 2.2 times larger negative thrust. This suggests that the use of opposite pitch has a potential to lower L/D and eliminate the mechanical air brakes. Regarding the efficiency, if the regeneration efficiency η is defined as

$$\eta = \frac{P}{FV}, \tag{45}$$

the opposite pitch propeller has 1.2 times better regeneration efficiency.

VIII. Conclusion

EA are attracting considerable attention as secure, efficient, and eco-friendly aviation. The electric motor enables power regeneration during descent, but keeping the desired descent angle requires the control of the windmilling propeller. In this study, the descent angle control method based on the negative thrust controller was proposed. In addition, it was discovered that the use of opposite pitch has a potential of eliminating the mechanical air brakes. The effectiveness of the proposed methods was verified by simulations and wind tunnel experiments.

Future works include auto-landing control and optimization of descent path to maximize the regeneration energy. Also, the regeneration capability of reverse pitch and other pitch angles can be tested and discussed.

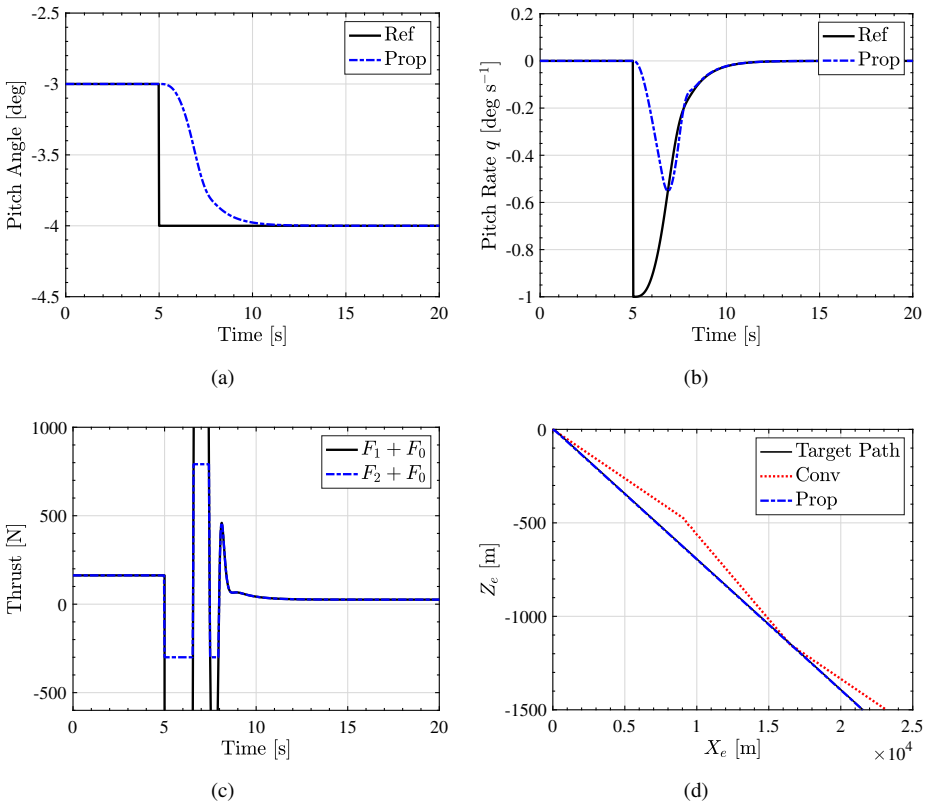

Fig. 8 (a) Step response of pitch angle. (b) Reference and output of pitch rate controller. (c) Control input F_1 and F_2. (d) Descent paths of conventional and proposed methods.

Acknowledgments

The authors would like to thank Mr. H. Kobayashi from Japan Aerospace Exploration Agency, for his valuable advice and technical assistance with the experiments. This research was partly supported by the Ministry of Education, Culture, Sports, Science, and Technology grant (grant number 18H03768 and 26249061).

References

[1] Nishizawa, A., Kobayashi, H., Okai, K., and Fujimoto, H., "Progress of Electric Vehicle Technology and Future of Electric Aircraft," *The 43rd JSASS Annual Meeting*, 2012.

[2] Hori, Y., "Future vehicle driven by electricity and control - Research on four-wheel-motored "UOT Electric March II"," *IEEE Transactions on Industrial Electronics*, Vol. 51, No. 5, 2004, pp. 954–962. https://doi.org/10.1109/TIE.2004.834944.

[3] Borer, N. K., Patterson, M. D., Viken, J. K., Moore, M. D., Bevirt, J., Stoll, A. M., and Gibson, A. R., "Design and Performance of the NASA SCEPTOR Distributed Electric Propulsion Flight Demonstrator," Tech. rep., 2016. https://doi.org/10.2514/6.2016-3920.

[4] Adachi, N., Kobayashi, H., Hakojima, H., and Nishizawa, A., "An Experimental Study on Energy Regeneration Using Propellers," Tech. rep., 2015.

[5] Takahashi, K., Fujimoto, H., Hori, Y., Kobayashi, H., and Nishizawa, A., "Airspeed control of electric airplane based on 2-quadrant thrust control and verification with towing test using electric vehicle," *40th Annual Conference of the IEEE Industrial Electronics Society*, IEEE, 2014, pp. 2682–2688. https://doi.org/10.1109/IECON.2014.7048885.

[6] Kobayashi, N., Fujimoto, H., and Kobayashi, H., "A study of Range Extension Control System by Optimization of Motor Torque and Propeller Pitch Angle for Electric Airplane," *IEE of Japan Technical Meeting Record*, 2013, pp. 6–11.

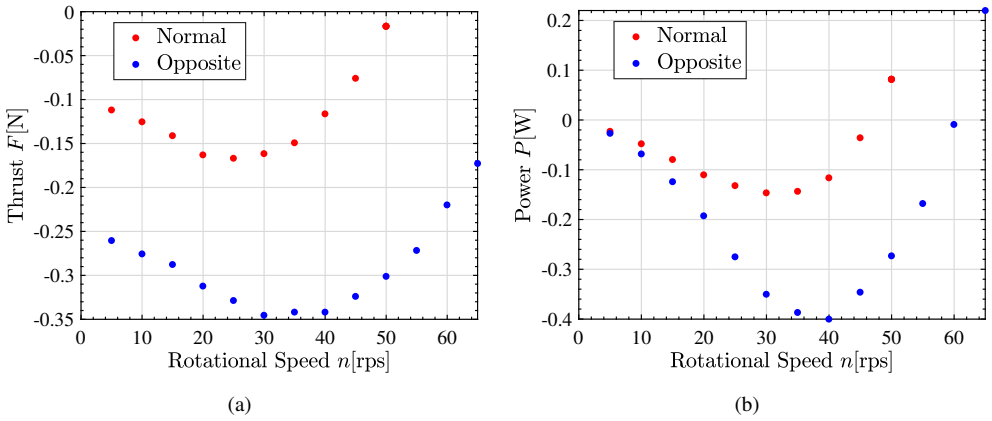

Fig. 9 APC 8×4 (a) The relation between rotational speed and thrust of normal and opposite pitch at $5.6\,\mathrm{m\,s^{-1}}$ airspeed. (b) The relation between rotational speed and regeneration power of normal and opposite pitch at $5.6\,\mathrm{m\,s^{-1}}$ airspeed.

[7] Konishi, N., Fujimoto, H., Kobayashi, H., and Nishizawa, A., "Range extension control system for electric airplane with multiple motors by optimization of thrust distribution considering propellers efficiency," *40th Annual Conference of the IEEE Industrial Electronics Society*, IEEE, 2014, pp. 2847–2852. https://doi.org/10.1109/IECON.2014.7048912.

[8] Fujimoto, H., and Sumiya, H., "Range extension control system of electric vehicle based on optimal torque distribution and cornering resistance minimization," *Industrial Electronics Conference*, IEEE, 2011, pp. 3858–3863. https://doi.org/10.1109/IECON.2011.6119939.

[9] Nodama, T., and Sunada, S., "An Investigation on Battery Charging with a Propeller," *Journal of the Japan Society for Aeronautical and Space Sciences*, Vol. 63, No. 1, 2015, pp. 8–12. https://doi.org/10.2322/jjsass.63.8.

[10] Okuyama, M., Nishizawa, H., and Kobayashi, A., "Aerodynamic Characteristics of Windmilling on Propeller," Tech. rep., 2015.

[11] Xiang, Y., Fujimoto, H., Hori, Y., Watanabe, Y., and Suzuki, K., "Proposal of Regeneration Power Control System by Optimization of Propeller Pitch Angle and Revolution Speed for Electric Airplanes," *IEE of Japan Technical Meeting Record*, 2015, pp. 121–126.

[12] Nishizawa, A., Kobayashi, H., and Fujimoto, H., "Development and flight demonstration of regenerative electric propulsion system for aircraft application," *Electric & Hybrid Aerospace Technology Symposium*, Vol. 1, Bremen Germany, 2015.

[13] McCormick, B. W., *Aerodynamics, Aeronautics and Flight Mechanics*, 2nd ed., John Wiley & Sons, Inc., 1995. https://doi.org/10.1177/095441009721100102.

[14] Yokota, K., Fujimoto, H., and Hori, Y., "Basic Study on Regenerative Air Brake Using Observer-based Thrust Control for Electric Airplane," *IEEE 16th International Workshop on Advanced Motion Control*, 2020. (accepted / to be presented).

[15] Kobayashi, H., Nishizawa, A., and Iijima, T., "Airspeed estimation by electric propulsion system parameters," *The 55st Aircraft Symposium*, 2017, pp. 869–878. https://doi.org/10.5545/sv-jme.2011.212.

[16] Kobayashi, H., Iijima, T., and Nishizawa, A., "Required Specifications of an Electric Propulsion System Based on Flight Test Using a Motor Glider," Tech. rep., Japan Aerospace Exploration Agency, 2015.

[17] Yoshida, Y., "Evaluation Mehods for Flight Handling Qualities of Small Aircraft," Ph.D. thesis, Hosei University, 2016.

[18] Asami, M., "Study on Measurement and Evaluation of Flying Quality of Light Aircraft," Ph.D. thesis, Hosei University, 2019.

[19] Kato, K., Oya, A., and Karasawa, K., *Basics of Aircraft Dynamics (in Japanese)*, University of Tokyo Press, 1982.

[20] JAXA, "Electric and hybrid propulsion system for aircraft," , 2020. URL http://www.aero.jaxa.jp/eng/research/frontier/feather/.

[21] Kouhei, O., Shibata, M., and Murakami, T., "Motion Control for Advanced Mechatronics," *IEEE/ASME Transactions on Mechatronics*, Vol. 1, No. 1, 1996, pp. 56–67. https://doi.org/10.1109/3516.491410.